Shock induced melting of sapphire

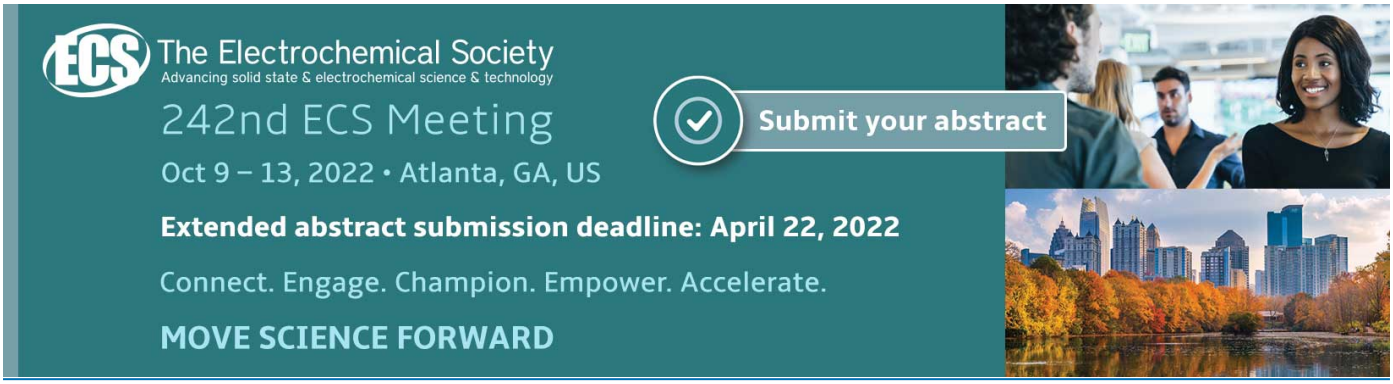

Journal of Physics: Conference Series **2154** (2022) 012010 doi:10.1088/1742-6596/2154/1/012010

Shock induced melting of sapphire

A Ostrik* **and D Nikolaev**

Laboratory of Equations of State of Matter, Institute of problems of chemical physics RAS, 1 Prospect Academician Semenov, 142432, Chernogolovka, Russian Federation

*E-mail: ostrik@ficp.ac.ru

Abstract. The method for calculation the melting curves of crystalline bodies based on the Debye model of heat capacity and the Lindemann melting rule is proposed. Hugoniot shock adiabate, determined in dynamic experiments and thermophysical characteristics of the substance under normal conditions are used as input data. Mathematically, the calculation of the melting curve is reduced to the Cauchy problem for a system of ordinary differential equations. This system is solved numerically by the Runge-Kutta method. Using the proposed method, the melting curves of copper, silver, gold, and sapphire at high pressures are calculated. The results obtained for copper, silver and gold were compared with available calculated and experimental data to validate the method. Experiments on shock compression of transparent sapphire samples were performed, using a Mach-type cumulative explosive generators. Investigated pressure range (280-1350 GPa) covered a region of shock-induced melting. The temperature of shock front was registered by fast optical pyrometer together with shock velocity. Particle velocity and pressure were obtained by impedance matching technique. Satisfactory agreement of calculated and experimental data on temperature of melting behind the shock wave front in sapphire was obtained.

1. Introduction

Melting, being a phase transition of the first order, changes the aggregate state and significantly affects the properties of the substance. Some characteristics (density, entropy, electrical conductivity, transparency) undergo a jump on the melting curve. The need for knowledge about melting at high pressures arises in the physics of shock waves (SW), solid state physics, geophysics, astrophysics, and in many fields of engineering science. In particular, knowledge of melting curves is required for a better understanding of planetary interiors and construction of their thermal models [1].

Many works are devoted to the problem of melting of crystalline substance in compressed state. To determine the melting curve of a substance under pressure, the following methods are mainly used:

- optical or X-ray detection of melting under static compression in a diamond anvil cell;
- observation of melting caused by SW in dynamic experiments (change of slope of the shock adiabate or the SW temperature vs. pressure dependence;
- construction of multiphase equations of state (EOS) with explicit description of the solid-liquid boundaries;
- ab initio and molecular dynamics calculations.

For some metals, for example copper, the agreement between the calculated and experimental data is quite good [2, 3], but for other transition metals (in particular, molybdenum), there is no consensus on the interpretation of the data available [4-6]. For a number of reasons, experimental studies on melting were mainly focused on copper, iron and some other transition metals, covering pressures over

10 GPa and temperatures above 1000 K. So, the melting curves of metals that are no less interesting for theory and practice, for example magnesium, manganese, gold, silver, zinc, cadmium, aluminum, indium and lead, have remained insufficiently studied even at relatively low pressures.

Sapphire is an important window material used in dynamic experiments at high pressures and temperatures. This is a rigid and transparent dielectric. The example of its application is fabrication of a cell for dynamic compression of Hydrogen, accompanied by the measurement of its electrical resistance [7, 8]. The question is very important: does the sapphire as a window material retain its properties at high pressures and temperatures, especially transparency and low electrical conductivity. Electrical conductivity is sensitive to the state of a substance and to its structure. In the conditions of dynamic experiments, it is difficult to understand whether sapphire is in a solid or liquid state, due to the lack of data on the melting curve of sapphire at high pressures.

In the paper a method is proposed for calculating the melting curves of crystalline bodies based on the Debye heat capacity model (in the case of metals, contribution of the electrons subsystem to heat capacity is also taken into account) and the Lindemann melting criterion. The shock adiabats (SA) determined in dynamic experiments and the thermophysical characteristics of a substance under normal conditions are used as the main experimental data. Mathematically, the problem is reduced to solving the Cauchy problem for a system of ordinary differential equations. The system is solved numerically by the Runge-Kutta method. Using the proposed calculation method, the melting curves of copper, silver, and gold at high pressures are constructed. The results obtained for copper, silver and gold are used to validate the method by comparing it with the available calculated and experimental data of other authors.

As already noted, one of the approach to study melting is dynamic experiments [9], where high pressures are produced by shock wave. Light gas gun was used to study Iron, [10], but it's possibilities is barely enough to observe shock-induced melting of refractory oxides [11]. Later, a laser shock waves were used to study oxides [12-15]. The techniques to indicate melting of shock-compressed substance is: to find a difference in Hugoniot of various crystallographic orientation samples, disappearing at melting [15], x-rays diffraction [16], or direct observation of the temperature of shock wave front [12-14]. In our case, the cumulative explosive generators, based on Mach reflection of shock waves was used to close the pressure range between gas gun and laser SW, temperature of SW front was registered by optical pyrometry. The experimental results obtained on melting of shock-compressed sapphire is compared with the Hugoniot temperatures and melting curve, calculated by proposed technique.

2. Construction of equations of state and calculation of melting curves in the compression region

The method of constructing the EOS. To constructing the EOS of a substance, experimental data on shock-compression is traditionally used in combination with data on its thermophysical properties, in particular, the dependence of the specific heat capacity on temperature and density. The equations of state are constructed in the form:

$$E = E(\rho,T) = E_c(\rho) + E_T(\rho,T) = E_c(\rho) + \int_0^T C_v(\rho,T)\,dT, \tag{1}$$

$$P = P(\rho,T) = P_c(\rho) + P_T(\rho,T) = P_c(\rho) + \Gamma(\rho,T)\rho E_T = \rho^2 \frac{dE_c}{d\rho}(\rho) + \Gamma(\rho,T)\rho\int_0^T C_v(\rho,T)\,dT, \tag{2}$$

where ρ is the density of substance; E, E_c, E_T are total, cold and thermal specific energies; P, P_c, P_T are total, cold and thermal pressures; $\Gamma = \Gamma(\rho,T)$ is Gruneisen function; $C_v(\rho,T)$ is specific heat capacity at a constant volume.

The EOS of the form (1), (2) includes two unknown functions $E_c = E_c(\rho)$ and $\Gamma = \Gamma(\rho,T)$ (the dependence of the specific heat capacity on density and temperature is considered known), which must

be constructed from the shock-wave data taking into account the the condition of thermodynamic compatibility:

$$\left(\frac{\partial E}{\partial(1/\rho)}\right)_T = T\left(\frac{\partial P}{\partial T}\right)_\rho - P. \tag{3}$$

Substituting (1) and (2) into (3), we obtain the equation for determining the Gruneisen coefficient

$$\left(\frac{\partial T E_T \Gamma}{\partial T}\right)_\rho - \frac{2}{T}(T E_T \Gamma) = \left(\frac{\partial E_T}{\rho\,\partial(1/\rho)}\right)_T. \tag{4}$$

Integrating (4) with the initial condition (taking into account that for $T \to 0$ and $C_V \to 0$)

$$\left.\frac{E_T \Gamma}{T}\right|_{T=0} = \lim_{T\to 0}\left.\frac{\partial C_v}{\partial T}\right|_{T=0} \frac{T^2}{2}\frac{\Gamma}{T} = \lim_{T\to 0}\left.\frac{\partial C_v}{\partial T}\right|_{T=0} \frac{\Gamma T}{2} = 0,$$

we get

$$\Gamma(\rho,T) = \frac{T}{\mathrm{E}_T(\rho,T)} \int_0^T \left(\frac{\partial E_T(\rho,T)}{\rho\,\partial(1/\rho)}\right)_T \frac{dT}{T^2} \tag{5}$$

For the Debye approximation, if

$$E_T(\rho,T) = e_T\left(\frac{\theta_D(\rho)}{T}\right) T = 3(R/\mu)\nu\, D(\theta_D(\rho)/T)\; T, \qquad D(\mathrm{x}) = \frac{3}{x^3}\int_0^x \frac{z^3 dz}{e^z - 1},$$

$$C_v(\rho,T) = C_v(\theta_D(\rho)/T) = 3(R/\mu)\nu\left[D(\theta_D(\rho)/T) - \theta_D(\rho)/T\, D'(\theta_D(\rho)/T)\right],$$

from (5) we get

$$\Gamma(\rho) = \Gamma_{00}(\rho) = -\frac{\partial \ln(\theta_D(\rho))}{\partial \ln(1/\rho)}, \tag{6}$$

where $\Gamma_{00}(\rho)$ is Gruneisen function at zero temperature; $D(\mathrm{x})$ is Debye function; $\theta_D(\rho)$ is Debye temperature function of density; μ is molecular weight of the elemental cell of the crystal; ν is number of atoms in the elementary cell of the crystal.

Thus, in accordance with (6), in the Debye approximation, the Gruneisen function does not depend on temperature, and the relation (6) itself ensures the fulfillment of the condition of thermodynamic compatibility.

In the more general case, taking into account the contribution of electronic component to the heat capacity, the specific internal energy is determined by relation

$$E_T(\rho,T) = T\, e_T\left(\frac{\theta_D(\rho)}{T}\right) + \frac{c_e T^2}{2}\left(\frac{\rho_0}{\rho}\right)^{\gamma_e}, \tag{7}$$

where c_e is coefficient of electronic thermal conductivity; γ_e is the electronic analogue of the Gruneisen coefficient. From (5) – (7) we get

$$\Gamma(\rho,T) = \frac{T}{E_T(\rho,T)}\left[\Gamma_{00}(\rho)\, e_T\left(\frac{\theta_D(\rho)}{T}\right) + \gamma_e \frac{c_e T}{2}\left(\frac{\rho_0}{\rho}\right)^{\gamma_e}\right]. \tag{8}$$

According to (8), taking into account the contribution of the electron heat capacity, the Gruneisen function depends on temperature and is given by the density functions $\theta_D(\rho), \Gamma_{00}(\rho)$, defined further in tabular form.

To determine the cold energy function $E_c = E_c(\rho)$, data on shock compressibility $P_H = P_H(\rho)$ are used. From the Hugoniot relations we get:

$$E - E_0 = \frac{1}{2}(P_H(\rho) + P_0)\left(\frac{1}{\rho_0} - \frac{1}{\rho}\right),$$

Using (1), we have

$$E_T(\rho, T_H(\rho)) = \psi(\rho) - E_c^*, \tag{9}$$

$$\psi(\rho) = \frac{1}{2}(P_H(\rho) + P_0)\left(\frac{1}{\rho_0} - \frac{1}{\rho}\right) + E_{T0}, \qquad E_{T0} = E_T(\rho_0, T_0), \qquad E_c^* = E_c(\rho) - E_c(\rho_0),$$

where $T_H(\rho)$ is temperature of shock compression.

Since the EOS is fulfilled on SA also, then

$$-\frac{dE_c^*}{d(1/\rho)} + \Gamma(\rho, T_H(\rho))\rho E_T(\rho, T_H(\rho)) = P_H(\rho). \tag{10}$$

For polycrystalline substance, the function $\Gamma_{00}(\rho)$ is calculated from known relation (t=0 is Landau-Slater theory; t=1 is Dugdale–McDonald theory; t=2 – free-volume theory; γ=2t / 3)

$$\Gamma_{00}(\rho) = -\left(\frac{2-t}{3}\right) - \frac{1}{2\rho}\frac{d^2}{d(1/\rho)^2}\left(\rho^{-\gamma}P_c(\rho)\right)\left(\frac{d}{d(1/\rho)}\left(\rho^{-\gamma}P_c(\rho)\right)\right)^{-1}, \; P_c(\rho) = -\frac{dE_c^*}{d(1/\rho)}. \tag{11}$$

From (8)-(11) we get a system of five ordinary differential equations to determine unknown density functions

$$\begin{cases} dE_c^*/d\rho = Y_1, \qquad dY_1/d\rho = Y_2, \\ \dfrac{dY_2}{d\rho} = \dfrac{2}{\rho^2}\left(\dfrac{t-7}{3} + \Gamma_{00}^f(\rho)\right)\left(\rho Y_2 + (2-\gamma)Y_1\right) + (3-\gamma)(2-\gamma)\dfrac{Y_1}{\rho^2}, \\ \dfrac{dT_H}{d\rho} = \dfrac{d\psi/d\rho - Y_1 - \left(\partial E_T/\partial\rho\right)_T}{\left(\partial E_T/\partial T\right)_\rho}, \qquad \dfrac{d\theta_D}{d\rho} = \dfrac{\theta_D}{\rho}\Gamma_{00}^f(\rho), \end{cases} \tag{12}$$

where Y_1, Y_2 are first and second derivatives of cold energy on density, and function $\Gamma_{00}^f(\rho)$ is calculated with relation (ε is ratio of thermal energy of electrons and atoms of crystal lattice)

$$\Gamma_{00}^f(\rho) = \frac{P_H(\rho) - \rho^2 Y_1}{\rho(\psi(\rho) - E_c^*)}(1+\varepsilon) - \varepsilon, \qquad \varepsilon = \frac{c_e T}{2e_T}\left(\frac{\rho_0}{\rho}\right)^{\gamma_e}.$$

Initial conditions for the system of equations (12) given at normal density $\rho = \rho_0$ (zero index is marking the values at normal conditions):

$$E_c^*\big|_{\rho=\rho_0} = 0, \quad Y_1\big|_{\rho=\rho_0} = \frac{P_0}{\rho_0^2} - \frac{\Gamma_0 \mathrm{E}_{T0}}{\rho_0}, \quad Y_2\big|_{\rho=\rho_0} = -\left.\frac{dP_H}{\rho^2 d\rho}\right|_{\rho=\rho_0} - \Gamma_0^2\frac{\mathrm{E}_{T0}}{\rho_0^2} - \frac{2}{\rho_0}Y_1\big|_{\rho=\rho_0}, \tag{13}$$

$$T_H\big|_{\rho=\rho_0} = T_0, \qquad \theta_D\big|_{\rho=\rho_0} = \theta_{D0} \tag{14}$$

First condition is obvious from the definition of E_c^*. Second condition follows from (10) at $\rho = \rho_0$. Third condition for second derivative can be obtained from the condition of tangency of the third order of SA and the isentrope) ($\left(\partial P/\partial\rho\right)_{H0} = \left(\partial P/\partial\rho\right)_{S0}$). Fourth and fifth conditions are obvious.

Systems of differential equations (12) with initial conditions (13), (14) are integrated numerically by the Runge-Kutta method of the fourth order of accuracy with a variable step in density.

Method for calculating melting curve. As a rule, the quality of the constructed EOS is justified first by comparison with the experimental data on shock compressibility. In the proposed approach, the shock compressibility is reproduced with any reasonable accuracy (with an error no more than the error of the experimental data), because it is used as input data. Thus it seems reasonable to calculate a melting curve from the EOS, and to compare it with the experimental data available.

The Lindemann melting rule is used to calculate the melting curves. The essence of the rule is the statement that melting occurs when the ratio of the mean-square deviation to the distance between neighbor atoms reaches a threshold value [17]. This physically clear rule was used in a number of works to calculate the melting curves of many metals (see, for example, [18-20]). A more general mathematical formulation of the Lindeman criterion is obtained on the basis of the classical approach of the average field potential [21]

$$T_m = const \times \rho^{-\frac{2}{3}} \theta_D^2(\rho), \tag{15}$$

where T_m is melting temperature.

From (15) we get

$$T_m = T_{m0} \times \left(\rho_{m0} / \rho\right)^{\frac{2}{3}} \theta_D^2(\rho), \tag{16}$$

where T_{m0} – is melting temperature at normal (atmospheric) pressure; ρ_{m0} is density of substance in solid state at T_{m0} and normal pressure.

According to (16) dependence $T_m = T_m(\rho)$ can be calculated if the function $\theta_D = \theta_D(\rho)$ is known (it is defined as a part of constructed EOS) and experimentally obtained density ρ_{m0} [22] and temperature T_{m0}. Eventually, based on EOS $P = P(\rho, T)$ and the relationship, included in the proposed EOS $\theta_D = \theta_D(\rho)$, the melting curve $T_m = T_m(\mathrm{P})$ is constructed in parametric form, with a density ρ as a parameter:

$$T_m = T_m(\rho), \qquad P = P(\rho, T_m(\rho)). \tag{17}$$

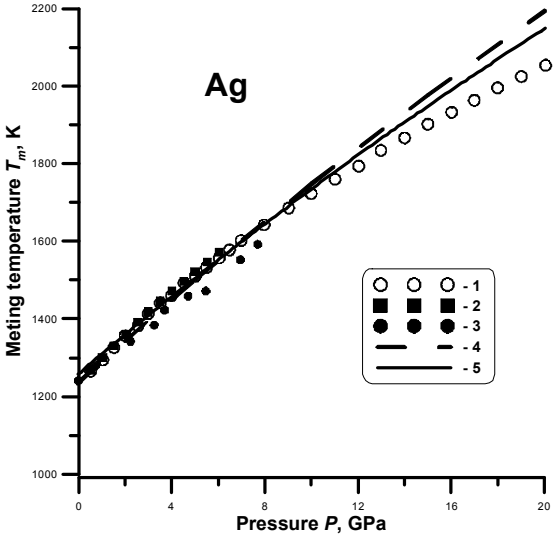

Figure 1. Melting curve of Silver. Experiments: 1-Akella 1971, DAC; [23]; 2-Mirwald 1979, DAC [24]; 3-Errandonea 2010, BTC [25]. Calculations: 4-Hieu 2013 [26]; 5- this work.

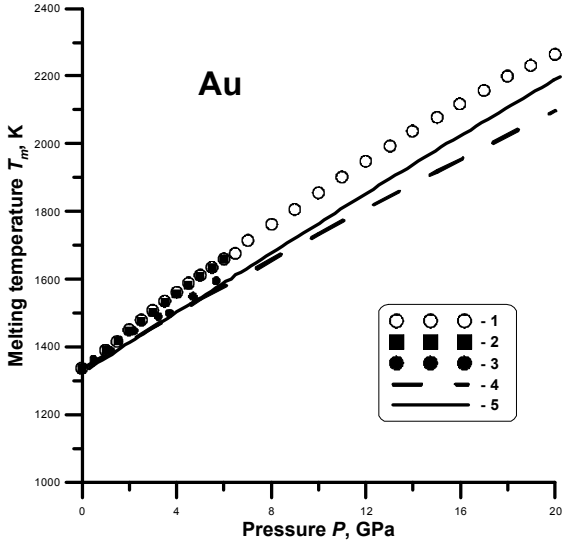

Figure 2. Melting curve of Gold. Experiments: 1-Akella 1971, DAC; [23]; 2-Mirwald 1979, DAC [24]; 3-Errandonea 2010, BTC [25]. Calculations: 4-Hieu 2013 [26]; 5- this work.

Melting curves of Silver and Gold. The noble metals Ag and Au are crystals with the fcc structure. The electronic configurations of its outer shells correspond to transition metal, $4d^{10}5s^1$ (Ag) and (Au) $5d^{10}6s^1$. Polymorphic transitions in Silver and Gold are not detected up to the pressures of megabar level. The absence of polymorphic transitions and relatively low melting temperatures (less than 1400 K) make these metals important for the study of melting physics. These metals are in many ways an ideal objects to compare results of theory and experiment.

Reliable experimental data obtained in diamond anvil cell (DAC) or Bridgman-type cell (BTC) are limited by low pressure levels. Comparison of these data with our calculations of melting curves in this pressure range is presented in figure 1-2. A satisfactory agreement of the data for silver is well seen. In the case of gold, the temperatures, obtained in the DAC [24] are higher than the results of calculations according to the Lindemann rule (this work and [26]).

Melting curve of copper. The chemical element Cu preserves the face-centered cubic structure (fcc) up to pressures above 100 GPa [26]. As already mentioned, this is one of the most studied transition metals, where there is a good coincidence of the melting data obtained by various methods. Therefore, copper can be used to compare various experimental methods and calculation models of melting at high pressures. Figure 3 presents a comparison of the results of our calculations with the theoretical and experimental data [23, 25-31].

It can be seen that in an extended pressure range, there is a noticeable difference in the calculated data above 100 GPa. Otherwise, in a range below 100 GPa, where experimental DAC data are available, the discrepancy between the results obtained by different methods seems insignificant. Our data are close to the data [27] obtained from constructing a wide-range EOS.

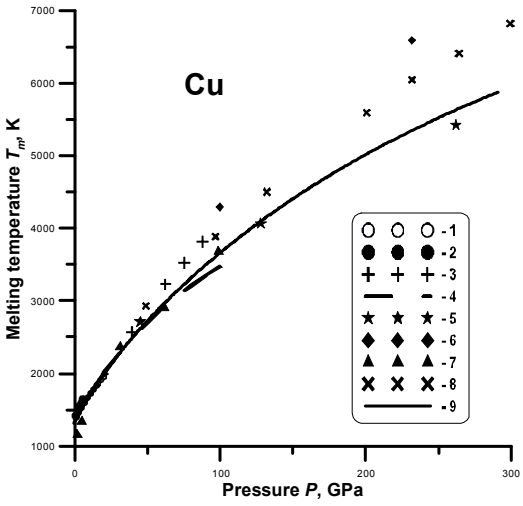

Figure 3. Melting curve of Copper. Experiments: 1- Akella 1971, DAC [23]; 2-Errandonea 2010, BTC [25]; 3-Japel 2005, DAC, [30]. Calculations: 4-Hieu 2014, [26]; 5-Urlin 1965, [27]; 6-Belonoshko 2000, MD-S, [28]; 7-Vokadio 2004, ab-inito, [29]; 8-Wu 2011, MD-S [31]; 9-this work.

The results of the comparison show that the developed approach is applicable for calculating the melting curves of crystalline bodies.

3. Experimental procedure

Cumulation (sometimes referred to as implosion) is well-known technique to raise parameters of explosive-driven shock wave generators. Explosive devices [32-34], utilizing the irregular Mach reflection of conical converging SW, are known from 1970th. The single reflection mode was realized, characterized by rapid pressure decrease behind Mach configuration. A slower attenuation of pressure can be obtained in device, proposed in [35], where a double Mach reflection is realized. Mach configuration is formed there in a layered cylindrical central body “hard shell-soft core", but the explosive charge and liner remain conical, as in [32-34], that considerably complicates the fabrication of device.

In [34], the complete rejection of conical parts in favor of cylindrical was proposed. In this case, a conical detonation wave is generated by sequential initiation of the main charge by a multipoint detonation distributor. Conical imploding liner, dynamically forming from cylindrical one, impacts the cylindrical central body of [35] type, producing a double Mach reflection configuration. More powerful generators were developed afterward on the basis of a small single-stage generator [36], characteristics are presented in Table 1. Even the small generator outruns the performance of light gas gun [37], where 340 GPa in sapphire was achieved. The pressure given in the table is a maximum performance,

but the pressure can be reduced within certain limits (about two times) by varying the geometry of the detonation distributor. The developed set of Mach generators provides a wide range of shock pressure from 2.5 Mbar to 17 Mbar.

The shock compressibility was measured by the impedance match technique [38]. The single crystal x-cut α-quartz was chosen as the reference material [39]. The temperature of SW front in sapphire was registered by an optical multichannel pyrometer [40] with fiber input. Pyrometer was calibrated using a standard tungsten ribbon lamp with known temperature and spectral emissivity.
The recording band of the pyrometer 500 MHz was sufficient for measuring the temperature in

Table 1. Characteristics of Mach type SW generators

	Type		
	Small single-stage	Big single-stage	Big double-stage
Diameter, mm	150	216	216
Length, mm	150	250	250
Mass of explosive charge, kg	3.9	12.5	12.5
Diameter of shock wave, mm	20 - 26	20	10
Maximum pressure in Quartz, GPa	295	520	1050
Maximum pressure in Sapphire, GPa	395	680	1320
Maximum pressure in Iron, GPa	490	860	1700

stationary parts of records with a length of 70-250 ns. Fast 2 GHz fiber-coupled photodetectors were used for precise measurement of time of SW passing through the reference and sample.

4. Results on Sapphire melting

Sapphire (Al_2O_3) is a molecular crystal and a dielectric with a band gap of 4.8 eV. Hence, the electronic part of the heat capacity is assumed as $c_e = 0$.

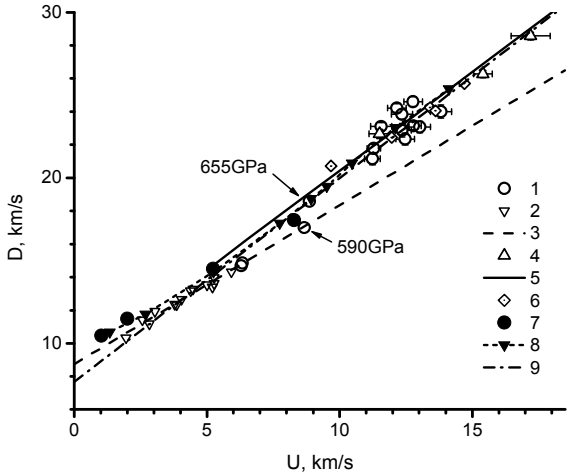

Figure 4. Sapphire shock compressibility. 1-this work, 2- [37], 3-linear fit of [37], 4–[41], 5–SESAME 7411 from [41], 6-[42, 43], 7-[44], 8-QMD calculation [45], 9-linear fit of [46].

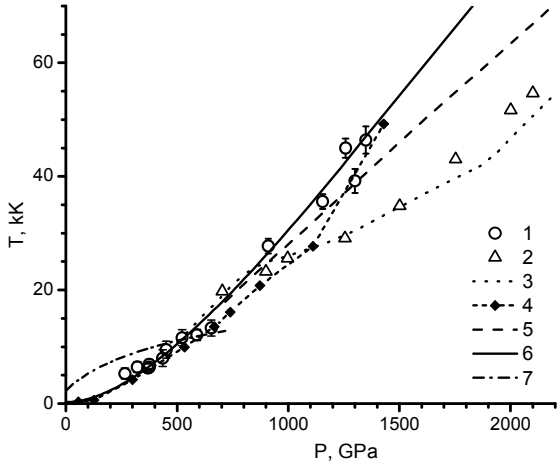

Figure 5. Sapphire temperature vs. shock pressure. Experiment: 1-this work, 2-[47]. Calculations: 3-[46]; 4-[45]; 5-SESAME 7411 (from [46]); 6-EOS model, this work; 7- EOS model, melting curve.

Experimental information on shock compressibility, required for the construction of EOS of Sapphire were taken from [37, 41] and data [44] taken from [43]. Our experimental data are presented in figure 4 (in coordinates shock velocity D vs. particle velocity U) together with the data [37, 41, 42], calculations [45,46], and SESAME – 7411 data from [41]. It's clear, that the our data in the range of

particle velocity of 11-14 km/s confirms the "stiff" course of the SA, indicated by points [41, 42]. The points in the region of U<10 km/s is in agreement with the data [37].

Thus, the Kerley approximation [46] works well in the entire region of interest

$$D = 7,673 + 1,23\ U \tag{18}$$

However, at low pressures, the experimental results better matches the Erskine's data [37] with a linear fit

$$D = 8,74 + U \tag{19}$$

To study the influence of the accuracy of the input shock compression data on EOS and melting curve, calculations were performed for SA (18) and a combination of (18) and (19):

$$D = \begin{cases} 8,74 + U, & U \le 4,639\ km/s \\ 7,673 + 1,23\ U, & U > 4,639\ km/s \end{cases} \tag{20}$$

The experimental data obtained in the work on the temperatures of shock compression of sapphire are presented in figure 5. In [41, 47], it was experimentally demonstrated, that the reflectivity of the SW front in sapphire can reach significant (up to R = 0.3 - 0.4) values, which corresponds to the emissivity ε = 0.7 – 0.6 and cause a noticeable difference between brightness and true temperatures. The reflectivity data [41, 47, 45] were used to process our temperatures for points with a pressure above 800 GPa (below 800 GPa reflectivity is negligible for temperature calculation). Coefficient of reflectivity R was determined by reflection of laser radiation at wavelength 532 nm, but the average wavelength in our experiments differs (900 nm), thus there can be inaccuracy, but reflectivity does not affect temperature obtained in a region of melting.

In [47] the temperature data includes the reflectivity of the front. Despite this, our raw brightness temperatures match the data [47]. If reflectivity is taken into account, temperature is increasing and corresponds well to the results of our EOS model. Also it is in a good agreement with the QMD calculation [45]. In [46] the pressure of 800 GPa stated as the onset of dissociation of sapphire melt. It should be noted that the experimental data obtained in this work are close to the calculated melting curve (curve 7 in figure 5).

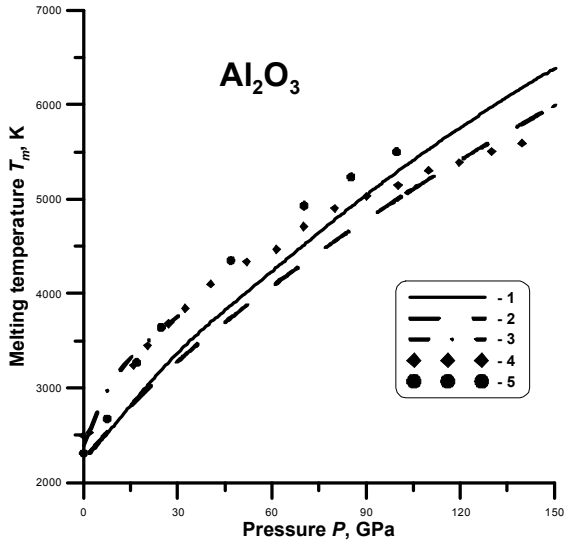

Figure 6. Sapphire melting curves at moderate pressures. 1-this work, bilinear fit (20); 2-this work, linear fit (18); 3-DAC [48]; 4-[49]; 5-MD-S [50].

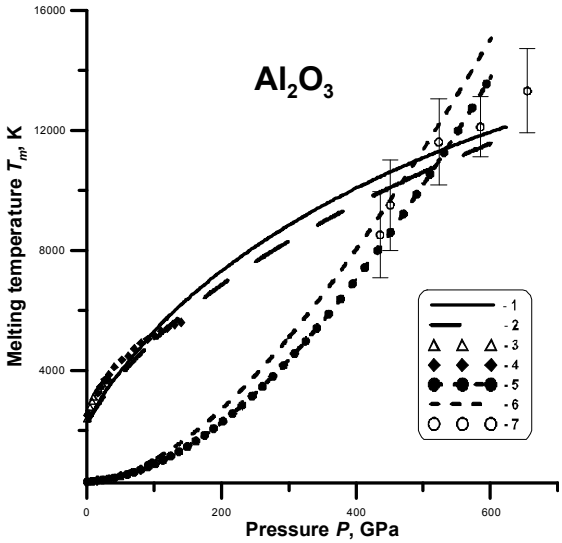

Figure 7. Sapphire melting at high pressures. Melting lines: 1-this work, bilinear fit (20), 2-this work, linear fit (18), 3-DAC [48], 4-[49]. Hugoniot temperatures, this work: 5-bilinear fit (20), 6-linear fit (18), 7- experiment.

Calculated melting curves of sapphire in comparison with the data available is presented at figures 6, 7. Additionally, figure 7 shows the Hugoniot temperature, calculated according to the proposed

EOS, where melting was not taken into account, and three experimental points melting region. At low pressures (figure 6), a satisfactory agreement of our calculations and the data [48-50] is observed. However, the slopes of the curves at the initial point (P=0), are very different, which is most probably due to the difference in the initial data for normal conditions. At pressures above 150 GPa, there is no experimental data on the melting curve of sapphire. Our melting curves was calculated for 2 various SA: bilinear D-U fit (20) and linear fit (18). Also, Hugoniot temperatures were calculated (figure 7). It seems, that bilinear fit is preferable for EOS calculation. Melting curve intersects with Hugoniot (see figure 7) at pressure of 500 GPa and a temperature of 11000 K, pressure is close to the data [41, 45]. Otherwise, onset of melting, declared in [46], is 400 GPa. From figure 7 it is clear, that above pressure of 500 GPa, experimental Hugoniot temperature changes slope and follows the calculated melting line within the measurement error. No indication of melting was observed experimentally near 400 GPa.

Conclusions

1. A new phenomenological approach to the construction of the EOS in the region of compression and to the calculation of the melting curves of crystalline substances at high pressures and moderate temperatures is proposed. The shock compression data, determined in dynamic experiments and the thermophysical characteristics of a substance at normal conditions are used as the input data.
2. The applicability of proposed approach to EOS construction is demonstrated by comparison with available calculated and experimental data on melting curves of silver, gold and copper in the megabar pressure range.
3. Using Mach shock wave generators, the Hugoniot of sapphire was experimentally refined in a pressure range below and above melting. Calculation of the melting curve of sapphire in high pressure region, where (at P > 150 GPa) the lack of data is observed, was carried out for two models of shock adiabate. The intersecting of calculated melting curve and Hugoniot provides a theoretical estimate of melting point of shock-compressed sapphire (500 GPa, 11000 K). Brightness temperature of the SW front in sapphire was measured in a wide range of pressures. The kink at experimental temperatures coincides with calculated melting line and indicates the onset of melting of sapphire.

Acknowledgments

Work is made with partial financial support from the Russian Foundation of Basic Researches (grant No. 19-08-00606-a).

The research was carried out within the state assignment AAA-A19-119071190040-5, thematic program No. 0089-2019-0001.

References

[1] Zharkov V N 1986 Interior Structure of the Earth and Planets (Harwood, New York)
[2] Japel S, Schwager B, Boehler R and Ross M 2005 *Phys. Rev. Lett.* **95** 167801
[3] Vocadlo L, Alfe D, Price G D and Gillan M J 2004 *J. Chem. Phys.* **120** 2872
[4] Errandonea D, Schwager B, Ditz R, Gessmann C, Boehler R and Ross M 2001 *Phys. Rev.* B **63** 132104
[5] Errandonea D J. 2006 *Phys. Chem. Solids* **67** 9–10 pp. 2017-2026
[6] Belonoshko A B, Burakovsky L, Chen S P, Johansson B, Mikhaylushkin A S, Preston D L, Simak S I and Swift D C 2008 *Phys. Rev. Lett.* **100** 135701
[7] Ternovoi V Ya, Pyalling A A, Nikolaev D N and Kvitov S V 2009 *AIP Conf. Proc.* **1195** 915
[8] Weir S T, Mitchell A C, Nellis W J 1996 *Phys.Rev.Lett* **76** 11 1860
[9] Altshuler L V, Trunin R F, Urlin V D, Fortov V E and Funtikov A I 1999 *UFN* **169** 3 323-344
[10] Ahrens T J, Tan H, Bass J. D 1990 *High Pressure Research* **2** 3 145
[11] Fat'yanov V, Asimow P 2014 *J. Phys.: Conf. Ser.* **500** 062003
[12] Root S, Shulenburger L, Lemke R W, Dolan D H, Mattsson T R, and Desjarlais M P. *Phys. Rev. Lett.* **115** 198501
[13] McWilliams R S, Spaulding D K, Eggert J H et al *Science* 2012 **338** 6112 1330

[14] Hicks D G,. Boehly T R, Eggert J H, Miller J E, Celliers P M and. Collins G W 2006 *Phys. Rev. Lett.* **97** 025502
[15] Duwal S, McCoy C A, Weck P F, Kalita P, Hanshaw H L, Cochrane K,. Ao T, and Root S 2020 *Phys. Rev B* **102**, 024105
[16] Turneaure S J, Sharma S M and Gupta Y M 2018 *Phys. Rev. Lett*. **121** 135701
[17] Lawson A C 2009 *Philosophical Magazine* **89** 1757
[18] Burakovsky L, Preston D L and Silbar R R 2000 *J. Appl. Phys.* **88** 6294
[19] Errandonea D 2005 *Physica* B **357** 356
[20] Arafin S, Singh R N, George A K 2013 *Physica B: Condensed Matter* **419** 40
[21] Wang Y. Ahuja R and Johansson B 2001 *Phys. Rev. B* **65** 014104
[22] Mao H K, Bell P M, Shaner J W and Steinberg D J 1978 *J. Appl. Phys*. **49** 3276
[23] Akella J and Kennedy G C 1971 *J. Geophys. Res.* **76** 20 4969
[24] Mirwald P W and Kennedy G C *1979 J. Geophys. Res: Solid Earth*, **84** (B12) 6750
[25] Errandonea D 2010 *J. App. Phys*. **108** (3) 033517
[26] Hieu H K 2013 *AIP Advances* **3** 112125
[27] Urlin V D 1966 *JETP* **22** 2 341
[28] Belonoshko A B, Ahuja R, Eriksson O and. Johansson B 2000 *Phys. Rev. B* **61** 3838
[29] Vocadlo L, Alfe O, Price G D, Gillan M J 2004 *J. Chem. Phys.* **120** (6) 2872
[30] Japel S, Schwager B, Boehler R and Ross M 2005 *Phys. Rev. Lett*. **95** 167801
[31] Wu Y N, Wang L P, Huang Y S, Wang D M 2011 *Chem. Phys. Lett*. **515** 4–6 217
[32] De Beaumont Ph and Leygonie L J 1970 *Proc. Fifth Intern. Symposium on Detonation* (Pasadena, CA, ACR-184 Office of Naval Research, Arlington, VA) 547
[33] Glushak B, Zharkov A et al. 1989 *ZETP* **96** 1301
[34] Derentowicz H 1989 *J. App. Mech. Tech. Phys.* **30** 1 21
[35] Zharkov A, Kryukov B 2004 *in: Physics of extreme states of matter, ed. V. Fortov et al*. (Chernogolovka, IPCP RAS), p.2.
[36] Nikolaev D, Ternovoi V et al. 2014 *J. of Physics Conference Series* **500** (14) 142026
[37] Erskine D 1994 *High-Press. Sci.* Techn.*-1993 ed. S. C. Schmidt et al*. (AIP Press NY) pp 141-143
[38] Zeldovich Y B, Raizer Y P 2002 *Physics of shock waves and high-temperature hydrodynamic phenomena* (Dover publications Inc. Mineola New York)
[39] Knudson M D and Desjarlais M P 2013 *Phys. Rev. B* **88** 184107
[40] Boslough M B and Ahrens T J 1989 *Rev. Sci. Inst*. **60** 3711
[41] Hicks D G, Celliers P M, Collins G W, Eggert J H and Moon S J 2003 *Phys.Rev. Lett.* **91** 035502
[42] Sano T et al. 2013 *Bull. Am. Phys. Soc*. **58** 28
[43] Ozaki N, Nellis W J et al. 2016 *Scientific Reports* **6** 26000
[44] Pavlovskii M N 1971 *Sov. Phys. Solid State* **12** 1737
[45] Liu H, Tse J S and Nellis W J 2015 *Scientific Reports* **5(1)** 12823
[46] Kerley G I 2009 *Report on contract 949182* (Johns Hopkins University, Applied Physics Laboratory, Laurel, MD)
[47] Miller J E 2006, *48th annual APS Meeting, division of Plasma physics.* Presentation is available at https://www.lle.rochester.edu/media/publications/presentations/documents/APS06/Miller_APS06.pdf
[48] Shen G, Lazor P 1995 *J. Gepophys. Res.* **100** B9 17699
[49] Wang Z, Mao H, Saxena S K 2000 *Journal of alloys and compounds* **299** 287
[50] Belonoshko A 1998 *Phys Chem Min* **25** 138